Spin-Canting-Induced Improper Ferroelectricity and Spontaneous Magnetization Reversal in $SmFeO_3$

Jung-Hoon Lee,[1] Young Kyu Jeong,[1] Jung Hwan Park,[1] Min-Ae Oak,[1] Hyun Myung Jang,[1,2,*] Jong Yeog Son,[3] and James F. Scott[4,†]

[1]*Department of Materials Science and Engineering, and Division of Advanced Materials Science, Pohang University of Science and Technology, Pohang 790-784, Republic of Korea*
[2]*Department of Physics, Pohang University of Science and Technology, Pohang 790-784, Republic of Korea*
[3]*Department of Applied Physics, College of Applied Science, Kyung Hee University, Suwon 446-701, Republic of Korea*
[4]*Department of Physics, Cavendish Laboratory, University of Cambridge, Cambridge CB3 0HE, United Kingdom*

(Received 11 May 2011; published 6 September 2011)

$SmFeO_3$, a family of centrosymmetric rare-earth orthoferrites, is known to be nonferroelectric. However, we have found that $SmFeO_3$ is surprisingly ferroelectric at room temperature with a small polarization along the *b* axis of *Pbnm*. First-principles calculations indicate that the canted antiferromagnetic ordering with two nonequivalent spin pairs is responsible for this extraordinary polarization and that the reverse Dzyaloshinskii-Moriya interaction dominates over the exchange-striction mechanism in the manifestation of the improper ferroelectricity. $SmFeO_3$ further exhibits an interesting phenomenon of spontaneous magnetization reversal at cryogenic temperatures. This reversal is attributed to the activation of the Sm-spin moment which is antiparallel to the Fe-spin moment below ~5 K.

DOI: 10.1103/PhysRevLett.107.117201 PACS numbers: 75.50.Ee, 71.15.Mb, 77.65.−j, 77.84.−s

Multiferroics exhibit simultaneous ferroic properties with coupled electric, magnetic, and structural orders. Over the past decade, there has been a resurgence of interest in understanding and applications of multiferroic materials [1–8]. A variety of theoretical models were proposed to account for the origin of magnetically induced ferroelectricity in antiferromagnetic oxides [9–16]. Among these, a spin-current-induction model [12] of the polarization of a $\mathbf{S}_i \times \mathbf{S}_j$ type in noncollinear magnets is particularly appealing as this model suggests the possibility of the occurrence of ferroelectricity in ABO_3-type orthoferrites which exhibit their canted antiferromagnetic (AFM) orderings well above room temperature [17,18]. According to this vector-field model based on the spin-orbit-coupling-driven reverse Dzyaloshinskii-Moriya interaction, a small improperlike polarization can appear in conjunction with a para-to-AFM transition in a centrosymmetric crystal having a noncollinear spin structure. Conversely, a ferroelectric distortion can induce spin-canted weak ferromagnetism [10] if the Dzyaloshinskii-type invariant [$\sim \mathbf{P} \bullet (\mathbf{M} \times \mathbf{L})$] is allowed in the free-energy expansion [15,19].

Accordingly, we have been exploring a suitable AFM material which is characterized by a noncollinear spin structure with its Néel temperature (T_N) substantially higher than 300 K and insulating property up to T_N. We find that $SmFeO_3$ (SFO hereafter), a family of rare-earth orthoferrites, meets these requirements. It is known to be antiferromagnetic below ~670 K [17] and is electrically resistive up to T_N. We will show that SFO is surprisingly ferroelectric with a substantial degree of the piezoelectricity at room temperature. On the basis of first-principles calculations, we conclude that the noncollinear AFM ordering with two nonequivalent spin pairs is primarily responsible for this extraordinary ferroelectricity. In addition to the magnetically induced ferroelectricity, SFO exhibits an interesting phenomenon of spontaneous magnetization reversal at cryogenic temperatures.

SFO is characterized by orthorhombic *Pbnm* (or *Pnma*) structure [Fig. 1(a)]. To understand the ground-state spin configuration of the Fe-spin subsystem, we have carried out density-functional theory (DFT) calculations on the basis of the generalized gradient approximation [20] implemented with the projector augmented wave pseudopotential [21] using the Vienna *ab initio* simulation package. According to the DFT calculations, the orthorhombic SFO is characterized by two nonequivalent canted AFM Fe-spin pairs, $(\mathbf{S}_2, \mathbf{S}_3) \equiv \alpha$ and $(\mathbf{S}_1, \mathbf{S}_4) \equiv \beta$, as schematically shown in Fig. 1(a). The ground-state AFM ordering direction (Néel vector) of each Fe-spin subsystem is predicted to be parallel to [001] of the *Pbnm* setting but with a small value of the net canted moment ($\mathbf{M}$) along [100]. More specifically, our DFT calculations predict the following relation for $\mathbf{M}$ (net magnetization of the Fe spin) in the Γ_2-spin structure [22] which is known to be stable for a wide temperature range including 300 K: $\mathbf{M} \equiv \mathbf{M}_\alpha + \mathbf{M}_\beta \equiv (\mathbf{S}_2 + \mathbf{S}_3) + (\mathbf{S}_1 + \mathbf{S}_4) = (0.076\hat{x} - 0.054\hat{y}) + (0.076\hat{x} + 0.054\hat{y}) = 0.152\hat{x}$, with $\mathbf{L}_\alpha \equiv (\mathbf{S}_2 - \mathbf{S}_3) = -7.10\hat{z}$ and $\mathbf{L}_\beta \equiv (\mathbf{S}_1 - \mathbf{S}_4) = +7.10\hat{z}$, where $\hat{x}$, for example, designates a unit vector along [100] (i.e., along the *a* axis), and $\mathbf{L}_\alpha$ and $\mathbf{L}_\beta$ denote the Néel vector for α and β subsystems, respectively [23]. Here numerical values are given in the unit of Bohr magneton (μ_B).

Fe $L_{2,3}$-edge x-ray magnetic circular dichroism (XMCD) spectra (ρ^+, ρ^-) of the flux-grown SFO single

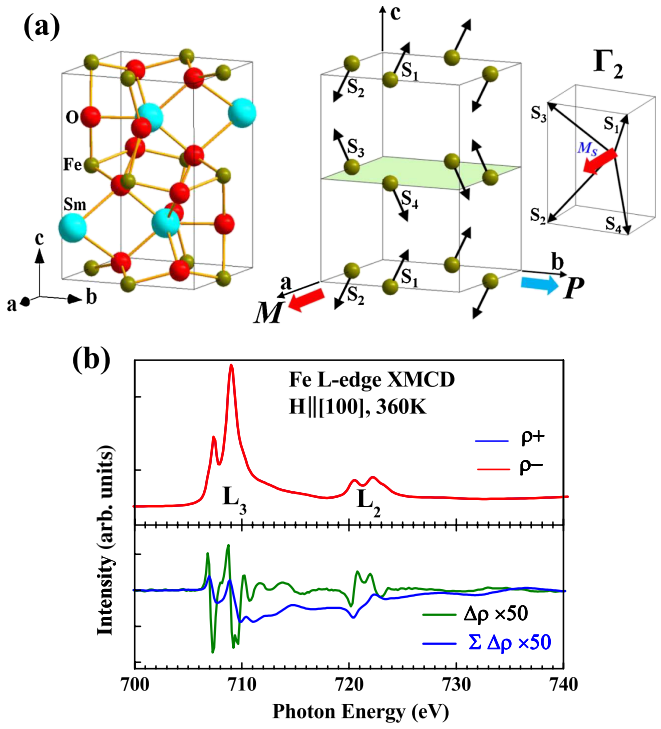

FIG. 1 (color online). Crystal structure and magnetic spectra of orthorhombic $SmFeO_3$. (a) A unit-cell crystal structure of $SmFeO_3$ in *Pbnm* setting (left) and a schematic Γ_2-spin structure showing two nonequivalent spin pairs (right). (b) Fe $L_{2,3}$-edge x-ray magnetic circular dichroism (XMCD) spectra obtained at 360 K. Bottom panel: MCD signals, $\triangle\rho$ and $\Sigma(\triangle\rho)$, over the entire $L_{2,3}$ region.

crystal [Fig. 1(b)] also demonstrate that the magnetic easy axis is parallel to [100] below T_{SR}. The four major dichroism ($\triangle\rho \equiv \rho^+ - \rho^-$) peaks that appeared at the L_3 region with two positive ($\triangle\rho > 0$) and two negative ($\triangle\rho < 0$) peaks indicate that two of the four nonequivalent spin moments ($\mathbf{S}_2, \mathbf{S}_3$) form one set of the spin subsystem ($\mathbf{M}_\alpha$) while the other two spin moments ($\mathbf{S}_1, \mathbf{S}_4$) form the other set of the spin subsystem ($\mathbf{M}_\beta$). Thus, the XMCD result supports the prediction of first-principles calculations. The integration of the dichroism over the entire $L_{2,3}$ absorption region [bottom panel of Fig. 1(b)] indicates that, unlike $GaFeO_3$ [24], the orbital magnetic moment of Fe ions is negligibly small, as compared with the spin magnetic moment.

The two prominent features of the magnetization-field (M-H) curve [Fig. 2(a)] are (i) a pronounced magnetic anisotropy and (ii) a small value of the coercive field ($\sim$30 Oe). These features can be practically exploited in the development of an ultralow-field magnetic switching device that requires an extremely small coercive field with a prominent anisotropy. The M-H curve also indicates that the magnetic easy axis of SFO is nearly parallel to the a axis of *Pbnm* (equivalently, parallel to the c axis of *Pnma*) [22]. This observation is consistent with our theoretical

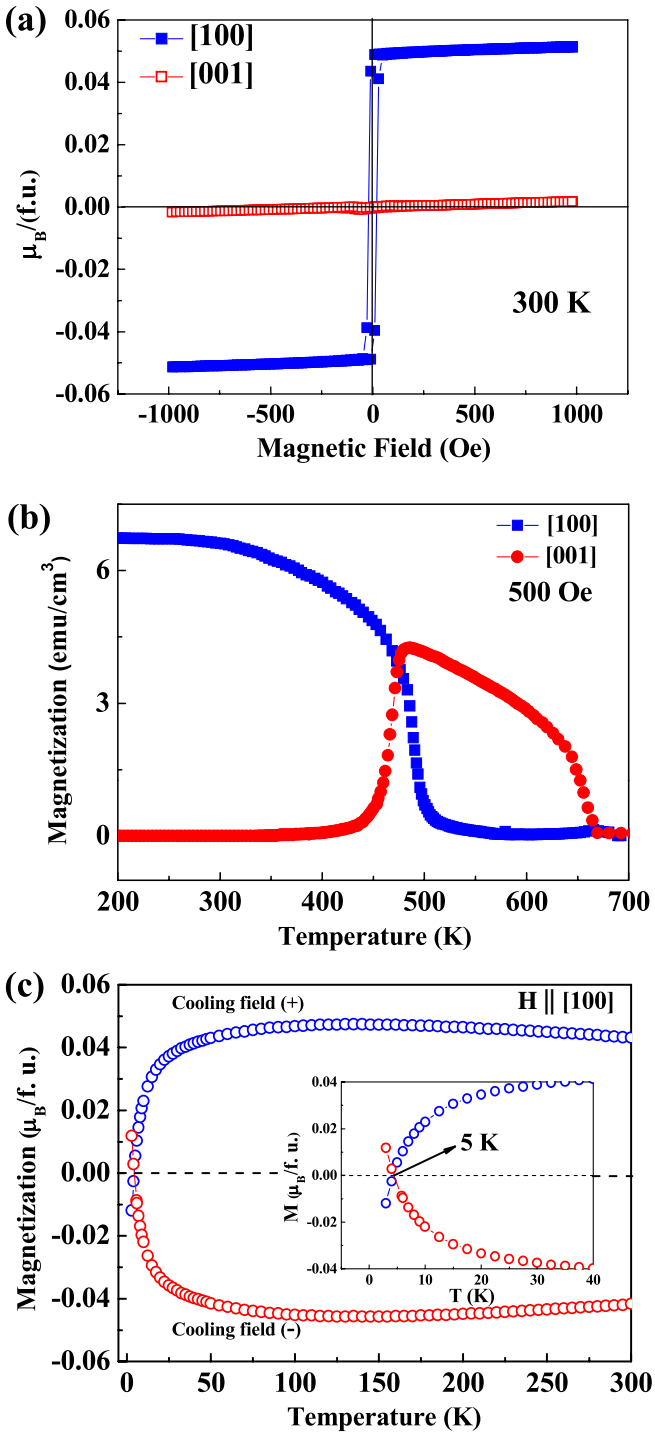

FIG. 2 (color online). Magnetic properties of the $SmFeO_3$ single crystal. (a) Room-temperature magnetization-field (M-H) hysteresis curves, showing the effect of the applied magnetic-field direction on the magnetization response. (b) Temperature-dependent magnetization, $M(T)$, curves showing a [001]-to-[100] spin-reorientation transition at $\sim$480 K. On the other hand, we did not find any meaningful [010] magnetization. (c) $M(T)$ curves for temperatures below 300 K, showing a thermally induced spontaneous magnetization reversal at 5 K. We measured $M(T)$ curves for both (+) and (−) cooling fields. The inset presents a magnified view of $M(T)$ at cryogenic temperatures.

prediction that $\mathbf{M} = 0.152\hat{x}$ for the Γ_2-spin structure, as discussed previously.

The temperature-dependent magnetization curve demonstrates an AFM ordering at 670 K (T_N). As shown in Fig. 2(b), there rapidly occurs a spin-reorientation (SR) transition at ~480 K, switching the magnetic easy axis of [100] to [001] with increasing temperature. This corresponds to a Γ_2-to-Γ_4 transition in the AFM spin configuration. According to our DFT calculations, $\mathbf{M}$ (the net magnetization of the Fe spin) in the Γ_4-spin structure, which is stable for the temperature range between T_N (670 K) and T_{SR} (480 K), is described by the following relation [23]: $\mathbf{M} \equiv \mathbf{M}_\alpha + \mathbf{M}_\beta \equiv (\mathbf{S}_2 + \mathbf{S}_3) + (\mathbf{S}_1 + \mathbf{S}_4) = (-0.045\hat{y} - 0.059\hat{z}) + (+0.045\hat{y} - 0.059\hat{z}) = -0.118\hat{z}$. This prediction is consistent with the observation of the [100]-to-[001] spin reorientation at T_{SR} [480 K; Fig. 2(b)].

Upon cooling to cryogenic temperatures, SFO further shows an interesting phenomenon of spontaneous magnetization reversal [Fig. 2(c)]. This suggests a long-range ordering of the rare-earth Sm^{3+}-spin moment. In this case, the direction of the net Sm^{3+} moment should be opposite to that of the canted Fe^{3+}-spin moment ($+a$) in the Γ_2-spin structure. According to our DFT calculations, the net magnetization is antiparallel to the a axis of $Pbnm$ with its value of $-0.061\mu_B$ per f.u. We are now able to delineate the evolution of the spin structure with decreasing temperature: (i) para-to-AFM ordering at 670 K (T_N), (ii) Γ_4-to-Γ_2 spin reorientation at 480 K, and (iii) spontaneous magnetization reversal caused by a long-range ordering of the rare-earth Sm^{3+}-spin moment along $-a$ of $Pbnm$. These sequential changes in the spin configuration with the variation of temperature are pictorially presented in Fig. 3.

Let us now examine the possibility of the occurrence of spin-canting-driven ferroelectricity. Since SFO is

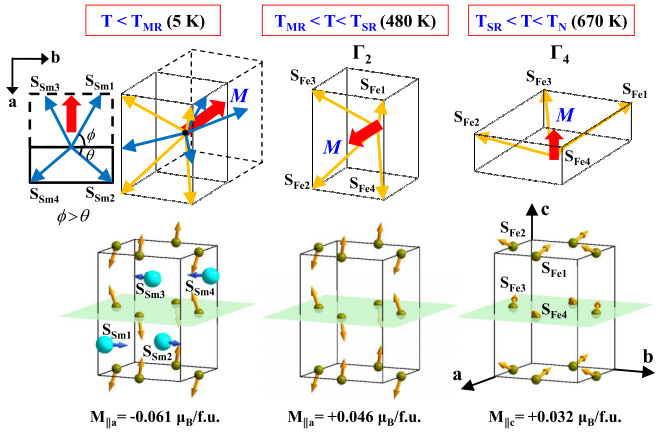

FIG. 3 (color online). Sequential changes in the spin configuration with the variation of temperature. The spontaneous magnetization reversal observed at 5 K (T_{MR}) is attributed to a long-range ordering of the Sm^{3+}-spin moment which is opposite to the canted Fe^{3+}-spin moment ($+a$) in the Γ_2-spin structure of orthorhombic $SmFeO_3$.

characterized by the two nonequivalent canted AFM subsystems, $\alpha = (\mathbf{S}_2, \mathbf{S}_3)$ and $\beta = (\mathbf{S}_1, \mathbf{S}_4)$, the noncollinear spin-canting-induced polarization has two distinct components, $\mathbf{P}_\alpha$ and $\mathbf{P}_\beta$, if they are nonzero. According to the spin-current-induction model [12], $\mathbf{P}_\alpha$ can be formally written as $\mathbf{P}_\alpha = \mathbf{e}_{23} \times (\mathbf{S}_2 \times \mathbf{S}_3)$. Our DFT computations using the Berry-phase method [25] now read: $\mathbf{P}_\alpha = \mathbf{e}_{23} \times (\mathbf{S}_2 \times \mathbf{S}_3) = +P_x\hat{x} - P_y\hat{y}$, where $P_x/P_y = 1.40$ and $P_y = +50.0\ \mu C/m^2$ for the Γ_2-spin structure. Similarly, DFT calculations predict: $\mathbf{P}_\beta = \mathbf{e}_{14} \times (\mathbf{S}_1 \times \mathbf{S}_4) = -P_x\hat{x} - P_y\hat{y}$. Thus, the net spin-canting-induced polarization ($\mathbf{P}_{ind} \equiv \mathbf{P}_\alpha + \mathbf{P}_\beta$), which is parallel to the b axis, is predicted to be $| -2P_y\hat{y} | = +100.0\ \mu C/m^2$ for the Γ_2-spin structure. Essentially the same prediction can be made for the Γ_4-spin structure which is known to be stable for the temperature range between T_{SR} and T_N: $\mathbf{P}_{ind} = \mathbf{P}_\alpha + \mathbf{P}_\beta = \{-P_y'\hat{y} - P_z'\hat{z}\} + \{-P_y'\hat{y} + P_z'\hat{z}\} = -2P_y'\hat{y}$ parallel to [010] with $P_z'/P_y' = 1.33$ [23]. Accordingly, we now deduce one important conclusion on the direction of $\mathbf{P}_{ind}$ that the net noncollinear spin-canting-induced polarization ($\mathbf{P}_{ind}$) remains to be parallel to [010], irrespective of the spin reorientation at T_{SR}.

Though the noncollinear spin-canting-induced polarization ($\mathbf{P}_{ind}$) corresponds to the reverse Dzyaloshinskii-Moriya interaction mechanism, it can be shown that the two Dzyaloshinskii-type invariants, i.e., $\{\mathbf{P}_\alpha \bullet (\mathbf{M}_\alpha \times \mathbf{L}_\alpha), \mathbf{P}_\beta \bullet (\mathbf{M}_\beta \times \mathbf{L}_\beta)\}$, cancel each other out [23] and, thus, do not contribute to the free-energy density, which is an interesting exception to Fennie's rule [15]. This indicates that a $\mathbf{P} \bullet (\mathbf{M} \times \mathbf{L})$-type trilinear coupling [19] is not effective in the orthorhombic SFO because of the presence of the two nonequivalent AFM subsystems.

Let us now consider experimental aspects of the canted AFM-ordering-induced ferroelectricity. The capacitance-voltage (C-V) hysteresis curve presented in Fig. 4(a) clearly demonstrates a nonzero remanent polarization (P_r) along the b axis of $Pbnm$ at 300 K. The magnitude of the induced polarization was evaluated by measuring and integrating temperature-dependent pyroelectric current [23]. As shown in Fig. 4(b), the polarization developed along the b axis of $Pbnm$ is ~93 $\mu C/m^2$. Figure 4(b) also shows that the onset of the para-to-ferroelectric transition coincides well with the AFM ordering temperature [670 K, Fig. 2(b)]. This strongly supports the AFM-ordering-induced ferroelectricity in a centrosymmetric crystal. A nonzero value of the spontaneous polarization (P_s) at 300 K was further confirmed by carrying out positive-up and negative-down (PUND) pulse measurement [23]. The saturation P_r value obtained from the PUND measurement at 300 K is ~100 $\mu C/m^2$, which coincides well with the DFT prediction of 100 $\mu C/m^2$ for the Γ_2-spin structure. The consistency between the DFT prediction (with the spin-orbit coupling option) and the experimental observation supports the prevalence of the noncollinear spin-orbit-coupling-driven polarization of a $\mathbf{S}_i \times \mathbf{S}_j$ type in SFO.

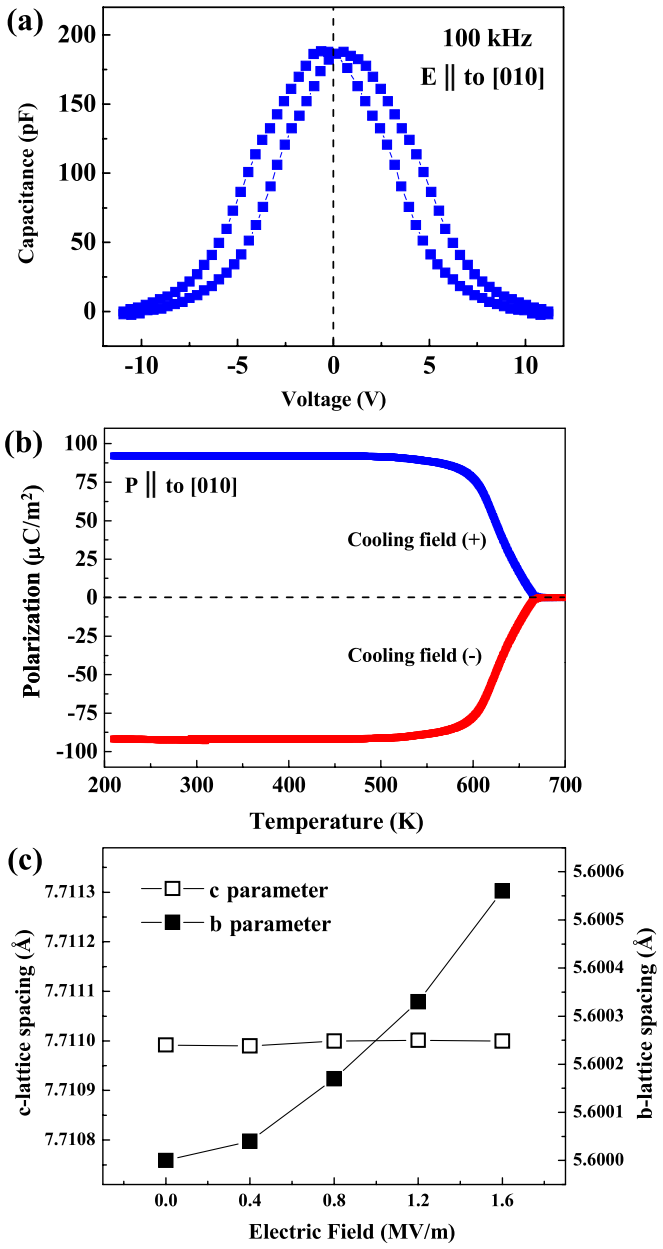

FIG. 4 (color online). Ferroelectric and piezoelectric responses of the $SmFeO_3$ single crystal. (a) A room-temperature C-V curve of the flux-grown orthorhombic $SmFeO_3$ single crystal obtained at a 100 kHz measuring frequency with the probing electric field along [010]. (b) Temperature-dependent spontaneous polarization along [010]. No pyroelectric response was detected for an electrically poled $SmFeO_3$ crystal along two other principal directions, [100] and [001]. (c) Variations of b- and c-axis parameters under the electric field applied to [010] and [001] directions, respectively.

On the other hand, the computed polarization is strictly zero if we do not adopt the spin-orbit coupling in the Berry-phase calculations. This clearly indicates that the exchange-striction mechanism of a $\mathbf{S} \bullet \mathbf{S}$ type [8] is not relevant to the manifestation of the improper ferroelectricity in SFO.

If SFO is truly ferroelectric, it should show a certain degree of the piezoelectricity along the P_s (spontaneous polarization) direction. To examine this proposition, we have carried out *in situ* synchrotron x-ray microdiffraction (XRMD) experiments [26]. According to the phenomenological thermodynamic prediction, the piezoelectric coefficient d_{22} (for both the elastic strain and the measuring field along the polarization direction, b axis of $Pbnm$) is nonzero while the other two diagonal components, d_{11} and d_{33}, should be nearly zero [23]. As shown in Fig. 4(c), the c-axis parameter evaluated using the branch of decreasing E field [26] is nearly independent of the applied E field, indicating that $d_{33} \approx 0$. We also found that $d_{11} \approx 0$. On the contrary, the slope is nonzero for d_{22}, and we have evaluated d_{22} using the XRMD data (for the linear low E-field region) and the relation $d_{22} = (\partial l_y/\partial E_y)_{T,\sigma=0}$, where l_y denotes the spontaneous elastic strain along the b axis. The estimated d_{22} ($\sim 22 \pm 4$ pm/V) is slightly higher than d_{33} of the epitaxial $BiFeO_3$ thin film (~ 15 pm/V) having 4 mm symmetry [26]. Thus, the XRMD study clearly supports that SFO is ferroelectric with its P_s along the b axis of $Pbnm$.

First-principles calculations indicate that the canted AFM ordering of a $\mathbf{S}_i \times \mathbf{S}_j$ type is primarily responsible for the observed extraordinary ferroelectricity in SFO. Thus, a high AFM ordering temperature with a noncollinear canted spin structure is the main reason why SFO is an ambient multiferroic while most other oxides are not.

This work was supported by the WCU (World Class University) program through the Korea Research Foundation funded by the Ministry of Education, Science and Technology (Grant No. R31-2008-000-10059-0). Computational resources provided by KISTI Supercomputing Center (Project No. KSC-2011-C1-03) of Korea are gratefully acknowledged.

*hmjang@postech.ac.kr
†jfs32@cam.ac.kr

[1] T. Kimura *et al.*, Nature (London) **426**, 55 (2003).
[2] N. Hur *et al.*, Nature (London) **429**, 392 (2004).
[3] T. Lottermoser *et al.*, Nature (London) **430**, 541 (2004).
[4] W. Eerenstein, N. D. Mathur, and J. F. Scott, Nature (London) **442**, 759 (2006).
[5] S.-W. Cheong and M. Mostovoy, Nature Mater. **6**, 13 (2007).
[6] S. Ishiwata, Y. Taguchi, H. Murakawa, Y. Onose, and Y. Tokura, Science **319**, 1643 (2008).
[7] T. Kimura, Y. Sekio, H. Nakamura, T. Siegrist, and P. Ramirez, Nature Mater. **7**, 291 (2008).
[8] Y. Tokunaga *et al.*, Nature Mater. **8**, 558 (2009).
[9] S. Goshen, D. Mukamel, H. Shaked, and S. Shtrikman, Phys. Rev. B **2**, 4679 (1970).
[10] D. L. Fox and J. F. Scott, J. Phys. C **10**, L329 (1977).
[11] D. V. Efremov, J. Van den Brink, and D. I. Khomskii, Nature Mater. **3**, 853 (2004).

[12] H. Katsura, N. Nagaosa, and A. V. Balatsky, Phys. Rev. Lett. **95**, 057205 (2005).
[13] M. Mostovoy, Phys. Rev. Lett. **96**, 067601 (2006).
[14] J. Hu, Phys. Rev. Lett. **100**, 077202 (2008).
[15] C. J. Fennie, Phys. Rev. Lett. **100**, 167203 (2008).
[16] S. Dong, R. Yu, J.-M. Liu, and E. Dagotto, Phys. Rev. Lett. **103**, 107204 (2009).
[17] E. N. Maslen, V. A. Streltsov, and N. Ishizawa, Acta Crystallogr. Sect. B **52**, 406 (1996).
[18] W. Slawiński, R. Przenioslo, I. Sosnowska, and E. Suard, J. Phys. Condens. Matter **17**, 4605 (2005).
[19] D. L. Fox, D. R. Tilley, J. F. Scott, and H. J. Guggenheim, Phys. Rev. B **21**, 2926 (1980).
[20] J. P. Perdew, K. Burke, and Y. Wang, Phys. Rev. B **54**, 16 533 (1996).
[21] G. Kresse and D. Joubert, Phys. Rev. B **59**, 1758 (1999).
[22] R. L. White, J. Appl. Phys. **40**, 1061 (1969).
[23] See Supplemental Material at http://link.aps.org/supplemental/10.1103/PhysRevLett.107.117201 for (i) two nonequivalent AFM subsystems and associated polarizations, (ii) thermodynamic analysis of piezoelectricity, and (iii) magnetodielectric effect.
[24] J. Y. Kim, T. Y. Koo, and J.-H. Park, Phys. Rev. Lett. **96**, 047205 (2006).
[25] R. D. King-Smith and D. Vanderbilt, Phys. Rev. B **47**, 1651 (1993).
[26] C. W. Bark, S. Ryu, Y. M. Koo, H. M. Jang, and H. S. Youn, Appl. Phys. Lett. **90**, 022902 (2007).